Rom J Morphol Embryol 2020, 61(4):1099–1109 ISSN (print) 1220–0522, ISSN (online) 2066–8279 doi: 10.47162/RJME.61.4.12

ORIGINAL PAPER

RJME Romanian Journal of Morphology & Embryology http://www.rjme.ro/

Biodistribution of essential oil-conjugated silver nanoparticles

OANA GHERASIM[1,2], ALEXANDRU MIHAI GRUMEZESCU[1,3], GEORGE DAN MOGOŞANU[4], BOGDAN ŞTEFAN VASILE[1], CORNELIA BEJENARU[5], LUDOVIC EVERARD BEJENARU[4], ECATERINA ANDRONESCU[1], LAURENŢIU MOGOANTĂ[6]

[1]*Department of Science and Engineering of Oxide Materials and Nanomaterials, Faculty of Applied Chemistry and Materials Science, Politehnica University of Bucharest, Romania*

[2]*Lasers Department, National Institute for Lasers, Plasma and Radiation Physics, Măgurele, Romania*

[3]*Research Institute of the University of Bucharest (ICUB), University of Bucharest, Romania*

[4]*Department of Pharmacognosy & Phytotherapy, Faculty of Pharmacy, University of Medicine and Pharmacy of Craiova, Romania*

[5]*Department of Pharmaceutical Botany, Faculty of Pharmacy, University of Medicine and Pharmacy of Craiova, Romania*

[6]*Research Center for Microscopic Morphology and Immunology, University of Medicine and Pharmacy of Craiova, Romania*

Abstract

The beneficial synergy between antimicrobial silver nanoparticles (AgNPs) and essential oils (EOs), with therapeutic effects that have been acknowledged and explored for a long time, opens the way towards developing new and promising alternatives for anti-infective therapies. With the aim to improve the cytocompatibility and stability of AgNPs and to overcome the volatilization of EOs, AgNPs conjugated with sage (*Salvia officinalis*) and cinnamon (*Cinnamomum aromaticum*) EOs were obtained in our study. The synthesis process was realized either by classical or ultrasound-assisted chemical reduction. Compositional and microstructural characterization of the as-obtained Ag@EO NPs was performed by X-ray diffraction (XRD), thermogravimetric analysis (TGA), scanning electron microscopy (SEM) and transmission electron microscopy (TEM). The biodistribution of Ag@EO NPs was evaluated on a mouse animal model.

Keywords: silver nanoparticles, essential oils, antimicrobial, biodistribution.

Introduction

The impressive use of silver (Ag)-based nanosystems in modern society includes various applications, such as environment protection [1–3], energetic industry [4–6], electronics [7–9], detection platforms [10–12], pharmacological products [13–15] and implantable devices [16–18]. In particular, excellent mechanical properties and optical behavior, as well as intrinsic biocompatibility and anti-pathogenic effects, are characteristics that recommend silver nanoparticles (AgNPs) to be used in the development of specific and effective unconventional biomedical applications. Their size- and morphology-related features, alongside a versatile surface chemistry with impressive biofunctionality, are responsible for their interactions with biological structures.

Even if incomplete and ambiguous data is available regarding the cytotoxic effects and antimicrobial mechanisms of AgNPs, the following events were reported to occur following their interactions with eukaryotes and prokaryotes: (*i*) structural and functional impairment of cellular membrane after electrostatically-guided interaction of constituent phosphate-/thiol-enriched cellular biomolecules with AgNPs; (*ii*) inactivation and denaturation of vital macromolecules and disruption of energy-dependent cellular events due to internalization of AgNPs and uptake of free Ag^+ ions; (*iii*) cellular oxidative damage due to intracellular formation of reactive oxygen species and free radicals [19–24].

Ag-based nanosystems represent a suitable choice to induce or potentiate the antimicrobial effects of clinically relevant biomedical materials and devices. Even if they possess remarkable therapeutic effects and intrinsic biocompatibility, relentless efforts were done to maximize the bioactivity of AgNPs and improve their stability. In this respect, a wide variety of capping agents and surface coatings were successfully evaluated, including inorganic or organic, natural or synthetic materials [25–28].

The classical chemical synthesis of AgNPs involves controlled electrochemical degradation of Ag salts in the presence of reducing agents and stabilizers [29, 30]. The process can be completed conventionally or by utilizing various external energy sources to conduct the chemical processes. The latter approach, known as the physicochemical synthesis of AgNPs, includes ultrasound-assisted synthesis [31, 32] and electromagnetic-assisted synthesis (performed in the presence of ultraviolet light, visible light, γ-radiation, and microwave radiation) [33–36].

Given the intrinsic therapeutic properties of plant-derived extracts, infusions and essential oils (EOs), their revaluation towards developing unconventional and effective pharmaceutical formulations is of great interest.

Their use as antimicrobial agents [37, 38], antioxidant systems [39, 40], anti-cancer platforms [41, 42] and wound dressings [43, 44] was reported.

Sage (*Salvia officinalis* L.) and cinnamon (*Cinnamomum aromaticum* Nees) EOs were herein selected for the synthesis of EO-conjugated AgNPs (Ag@EO NPs). Depending on several environmental conditions and plant-related developmental factors, distinctive constituents were identified in sage EO. Thujone, camphor and eucalyptol were reported as major components that proved responsible for the bactericidal and antibiofilm activity of sage EO against various Gram-positive and Gram-negative pathogens [45–47]. The broad-spectrum antibacterial efficiency of cinnamon EO against drug-susceptible and drug-resistant bacteria is related to its major constituents, cinnamaldehyde and eugenol, which were reported to synergize and impair cellular membrane and interfere with vital cellular processes [48–50].

Aim

In the present study, AgNPs were *in situ* conjugated with sage and cinnamon EOs, either by classical or ultrasound-assisted chemical reduction. We aimed to investigate the physicochemical features of Ag@EO NPs and to evaluate the impact of selected EOs and synthesis methods on their *in vivo* distribution.

Materials and Methods

Materials

The reagents required for the synthesis of Ag@EO NPs were purchased from Sigma-Aldrich (Merck Group, Darmstadt, Germany). All reagents were of analytical purity and used without further purification. Sage and cinnamon EOs were provided by a local supplier.

Synthesis of Ag@EO NPs

The chemical reduction of metallic salt (silver nitrate, $AgNO_3$) was employed to obtain the Ag@EO NPs. For each experimental batch, two solutions were prepared, namely: (*i*) metallic precursor solution, obtained by dissolving $AgNO_3$ in ultrapure water under magnetic stirring, at room temperature; and (*ii*) reducing-stabilizing solution, obtained by mixing D-glucose, sodium hydroxide and EO in ultrapure water under vigorous magnetic stirring, at 80ºC. The first solution was added drop by drop within the organic solution. The synthesis process was completed either under magnetic stirring (Ag@S and Ag@C samples) or in ultrasonic bath (Ag@SU and Ag@CU samples). The filtered precipitates were washed three times with ultrapure water then dried at room temperature. The as-obtained powdery samples were subjected to compositional and microstructural analysis and biological evaluation.

Characterization of Ag@EO NPs

X-ray diffraction (XRD)

The purity and cristallinity of all experimental powders were investigated using an XRD-6000 diffractometer from Shimadzu (Duisburg, Germany). All scans were recorded at room temperature, using $Cu_{K\alpha}$ radiation (λ = 1.056 Å) for diffraction angles between 10–70º.

Thermogravimetric analysis (TGA)

Small amounts from each Ag@EO powdery sample were subjected to thermal treatment in normal atmosphere, from room temperature to 1000ºC, at a heating rate of 1ºC/min. A DTG-TA-50H equipment from Shimadzu (California, USA) was used in this respect.

Scanning electron microscopy (SEM)

Initial data on the microstructure of EO-conjugated samples were obtained using the secondary electron beam (30 keV energy) of a Quanta Inspect F scanning electron microscope from FEI (Thermo Fischer Scientific, Oregon, USA). Before analysis, all samples were capped with a thin gold layer.

Transmission electron microscopy (TEM)

The intimate microstructure of EO-conjugated samples was investigated with a Tecnai™ G2 F30 S-TWIN transmission electron microscope equipped with selected area electron diffraction (SAED) accessory (FEI, Thermo Fischer Scientific). Before analysis, serial ethanol dilutions were obtained from each sample.

In vivo distribution of Ag@EO NPs

To evaluate the *in vivo* effects of synthesized NPs, three months old BALB/c mice were used as an animal model. Sterile volumes of 100 µL from each Ag@EO NPs suspension (1 mg/mL in ultrapure water) were administered into the jugular vein after anesthetization. Same volumes of saline solution were inoculated for control animals. All experiments were performed in duplicate. At two and 10 days after inoculation, general anesthesia was applied, followed by animal euthanasia and vital organs collection. The harvested organs (brain, myocardium, lung, liver, kidney, pancreas, and spleen) were treated with phosphate-buffered saline (PBS), preserved in 10% neutral buffered formalin (72 hours, room temperature) and prepared for paraffin processing. The resulted tissue fragments were treated with Hematoxylin (affinity for basophilic structures) and Eosin (affinity for acidophilic structures) staining protocol (HE). The as-obtained histological slides were examined with a Nikon Eclipse 55i binocular microscope (Apidrag, Bucharest, Romania) coupled with a high-resolution Nikon DS–Fi1 camera from Apidrag. Optical micrographs were collected and processed by using the Image-Pro Plus 6.0 software (Media Cybernetics, Buckinghamshire, UK).

Results

Characterization of Ag@EO NPs

The X-ray diffractograms of obtained powders are included in Figure 1. Regardless of the type of EO and synthesis conditions, intense diffraction maxima at 2θ values of 38.2º, 44.3º and 64.5º were identified for all samples. In compliance with PDF No. 00-004-0783, the peaks correspond to (1 1 1), (2 0 0) and (2 2 0) diffraction planes of face-centered cubic (fcc) crystalline Ag. In the case of samples obtained with sage EO (Ag@S and Ag@SU), the presence of narrow peaks indicated bigger

crystallite sizes than for NPs conjugated with cinnamon EO. Using the Scherrer formula, the crystallite size was calculated as follows: 25.24 nm (Ag@S), 28.40 nm (Ag@SU), 12.30 nm (Ag@C) and 12.51 nm (Ag@CU).

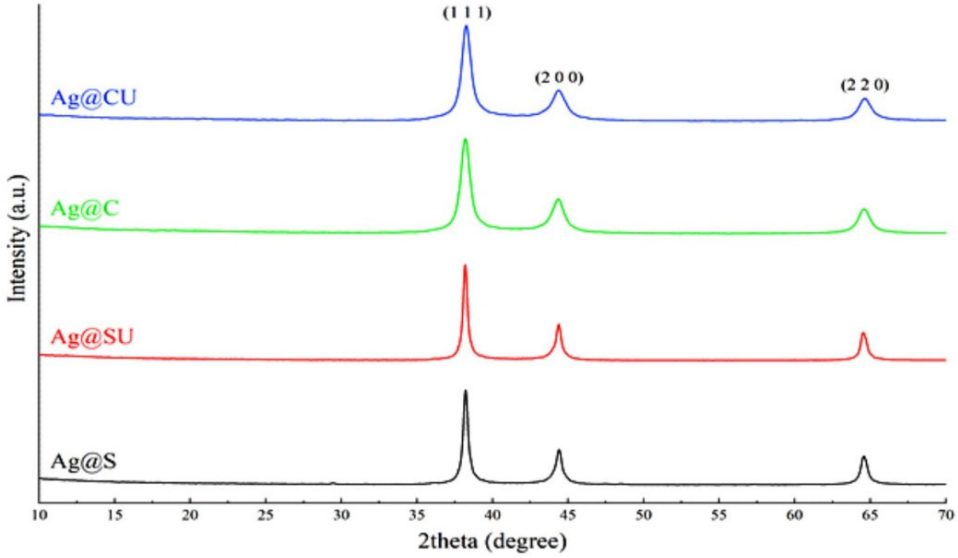

Figure 1 – ***X-ray diffractograms of Ag@EO NPs. Ag@EO NPs: Essential oil-conjugated silver nanoparticles.***

The thermal behavior of Ag-based powdery samples significantly depended on the type of EO used during synthesis (data not shown). In the case of AgNPs obtained in the presence of sage EO, a total weight loss of 2.443% and 1.824% was observed for Ag@S and Ag@SU, respectively. These results indicated the predominant metallic character of particles and the reduced amount of organic molecules conjugated onto the surface of these particles. In comparison, in the case of AgNPs synthesized in the presence of cinnamon EO, a total weight loss of 48.339% and 40.625% was obtained for Ag@C and Ag@CU, respectively, which indicated an increased amount of cinnamon EO molecules conjugated onto the surface of the metallic particles. Regardless of the type of EO, the mass loss occurred as follows: (*i*) chemo-desorption of surface water molecules (below 200ºC); (*ii*) evaporation and thermal degradation of abundant phytochemicals, namely monoterpenes and sesquiterpenes from sage EO and predominant phenylpropanoids and monoterpenes from cinnamon EO (between 200–400ºC); and (*iii*) thermal degradation of other terpenes from EOs' composition (above 400ºC) [51, 52].

Initial microstructural information about the synthesized NPs was provided by SEM analysis (Figure 2). Aggregates of nanosized particles with a preferential spherical morphology were noticed, with only a few rod-shaped NPs being observed for the samples conjugated with sage EO. NPs of ~30 nm and ~20 nm were obtained when using sage (Ag@S, Ag@SU) and cinnamon (Ag@C, Ag@CU) EOs, respectively. Also, SEM micrographs evidenced that the use of cinnamon EO led to the formation of smaller NPs.

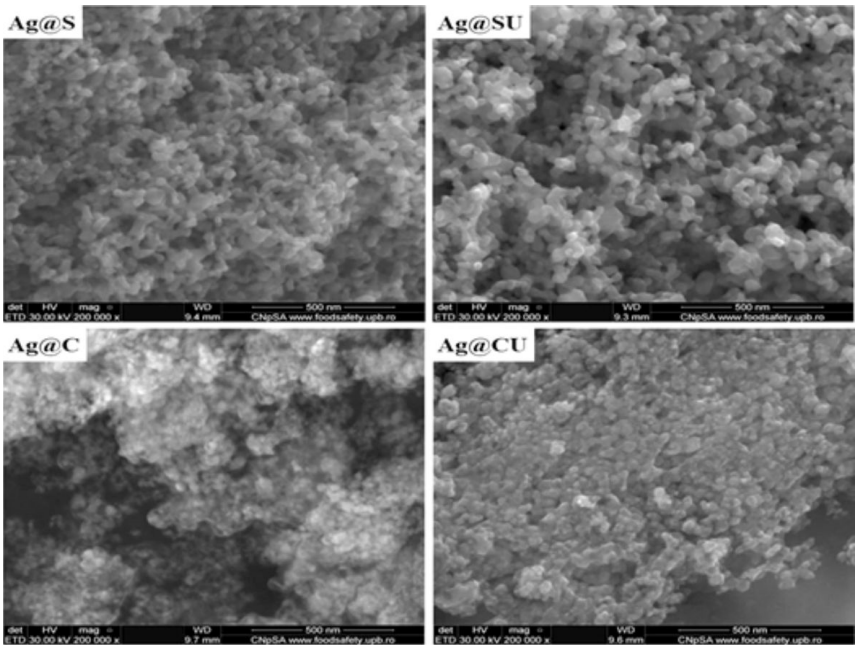

Figure 2 – ***SEM micrographs of Ag@EO NPs. Ag@EO NPs: Essential oil-conjugated silver nanoparticles; SEM: Scanning electron microscopy.***

TEM micrographs from Figure 3 reinforced the SEM analysis, with regards to the spherical morphology of all the synthesized EO-conjugated NPs, with few rod-shape NPs in the case of Ag@S and Ag@SU samples. The estimated physical particle size was determined as follows: ~25 nm (Ag@S), ~27 nm (Ag@SU), ~16 nm (Ag@C) and ~19 nm (Ag@CU). Regardless of the type of EO and the synthesis method, the high-resolution TEM (HR-TEM) images evidenced a core/shell structure for all NPs, with a uniform organic layer of ~2 nm and ~5 nm being noticed for NPs obtained by conventional reduction (Ag@S, Ag@C) and ultrasound-assisted synthesis (Ag@SU, Ag@CU), respectively. Also, the inset SAED patterns evidenced the presence of (1 1 1), (2 0 0), (2 2 0) and (3 1 1) diffraction planes of fcc Ag.

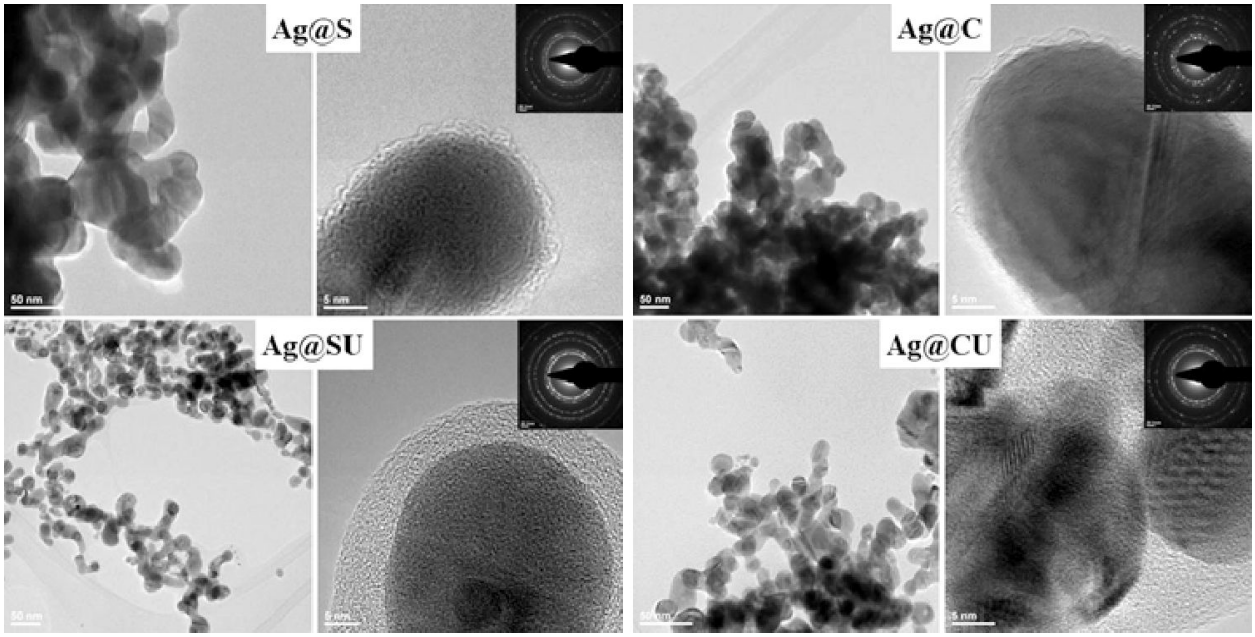

Figure 3 – ***TEM micrographs of Ag@EO NPs. Ag@EO NPs: Essential oil-conjugated silver nanoparticles; TEM: Transmission electron microscopy.***

In vivo distribution of Ag@EO NPs

After systemic administration of Ag@EO NPs and subsequent histological examination, preferential tissue retention of synthesized NPs was evidenced.

No morphological alterations or ultrastructural modifications were noticed in the brain (Figure 4), myocardium (Figure 5) and pancreas (Figure 6) tissues, regardless of the testing time. Typical histological aspects were identified in these tissue fragments, namely (*i*) cells with prominent vesicular nuclei in the transverse sections of brain tissues, (*ii*) striated muscle fibers with oval-to-round nuclei in the longitudinal sections of cardiac tissues, (*iii*) polarized epithelial cells with central spherical nuclei within the pancreatic acini (exocrine pancreas) and well-defined and normal Langerhans islets (endocrine pancreas). Few arterioles and venules containing normal erythrocytes were observed for these tissue fragments, indicating preserved blood vessel integrity. Moreover, no foreign structures were identified in any of these tissues.

In the case of hepatic (Figure 7) and pulmonary (Figure 8) tissues, dark-brown aggregates were present within tissue-specific resident macrophages, but isolated reduced-in-size aggregates were also identified within local blood vessels. A time-dependent tissue distribution of Ag@EO NPs was noticed. Even if such aggregates were identified within hepatic stellate macrophages (Kupffer cells) after both treatment times, the normal ultrastructure of liver tissues was not affected. The optical micrographs of lung sections evidenced the presence of Ag@EO NPs aggregates within pneumocytes and alveolar macrophages. Higher tissue distribution was noticed with longer treatment (10 days), accompanied by increased alveolar breakdown and inflammatory infiltrate. Smaller aggregates were observed for Ag@SU and Ag@CU samples.

A particular distribution of Ag@EO NPs was observed in the case of renal tissues (Figure 9). Regardless of the type of EO and the synthesis method, dark-brown aggregates were identified after both testing times, their presence being exclusively evidenced in the blood vessels. It was clearly observed that Ag@EO NPs aggregates were smaller and had a significantly reduced presence after 10 days. No morphological and ultrastructural alterations were noticed for renal glomeruli, tubules and stroma.

Major modifications were observed for splenic tissues (Figure 10), both at two and 10 days after injection. Ag@EO NPs aggregates were identified in a time-dependent manner within the splenic red pulp. Even if no foreign structures were noticed within the white pulp of the spleen, significant hypertrophy was observed. This was due to Ag@EO NPs-activated overproduction of multilobed nucleated macrophages.

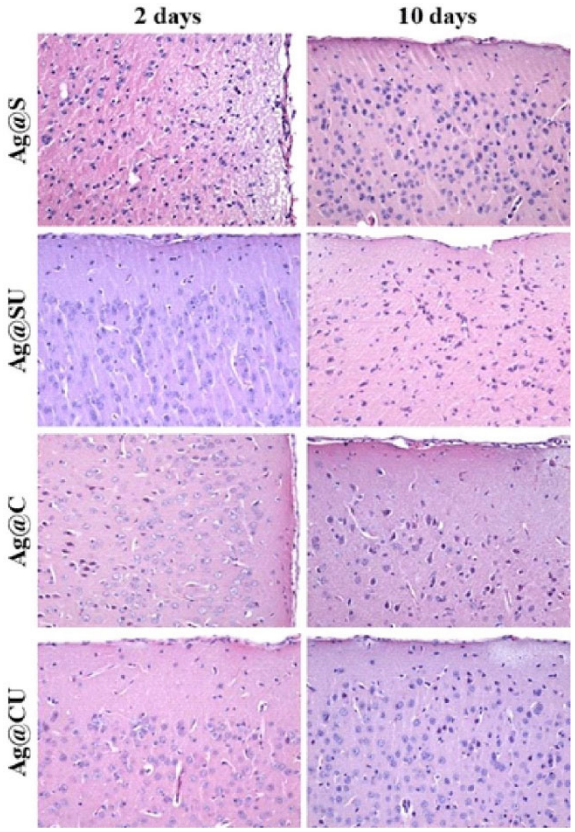

Figure 4 – ***Optical micrographs of brain tissues after two and 10 days of treatment with Ag@EO NPs (HE staining, 200×). Ag@EO NPs: Essential oil-conjugated silver nanoparticles; HE: Hematoxylin–Eosin.***

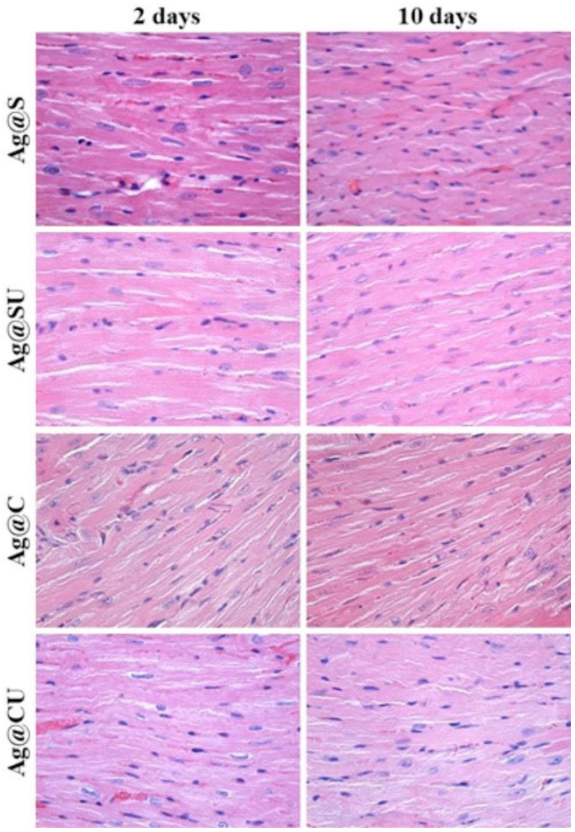

Figure 5 – ***Optical micrographs of cardiac tissues after two and 10 days of treatment with Ag@EO NPs (HE staining, 400×). Ag@EO NPs: Essential oil-conjugated silver nanoparticles; HE: Hematoxylin–Eosin.***

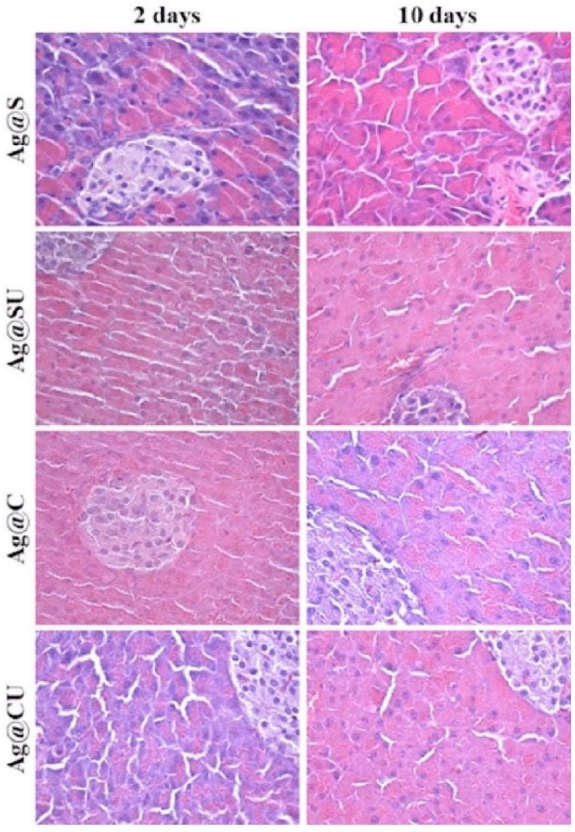

Figure 6 – ***Optical micrographs of pancreatic tissues after two and 10 days of treatment with Ag@EO NPs (HE staining, 400×). Ag@EO NPs: Essential oil-conjugated silver nanoparticles; HE: Hematoxylin–Eosin.***

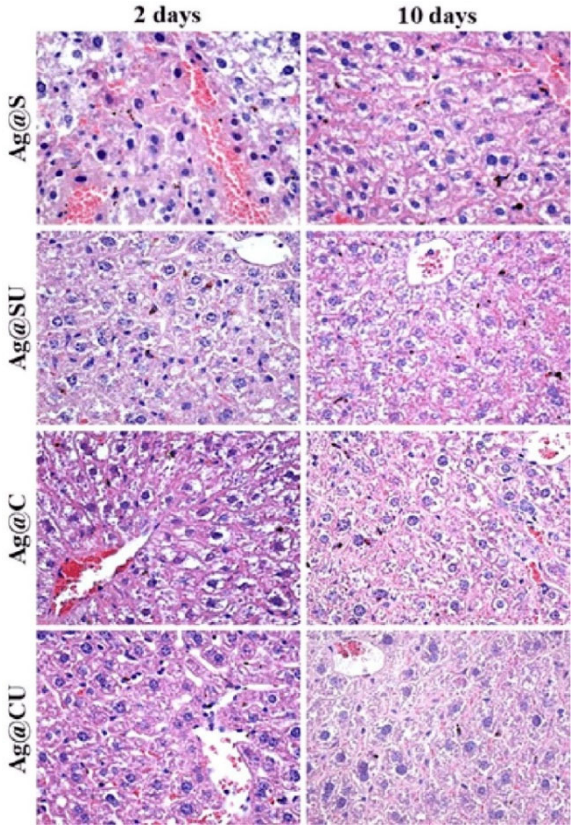

Figure 7 – ***Optical micrographs of hepatic tissues after two and 10 days of treatment with Ag@EO NPs (HE staining, 400×). Ag@EO NPs: Essential oil-conjugated silver nanoparticles; HE: Hematoxylin–Eosin.***

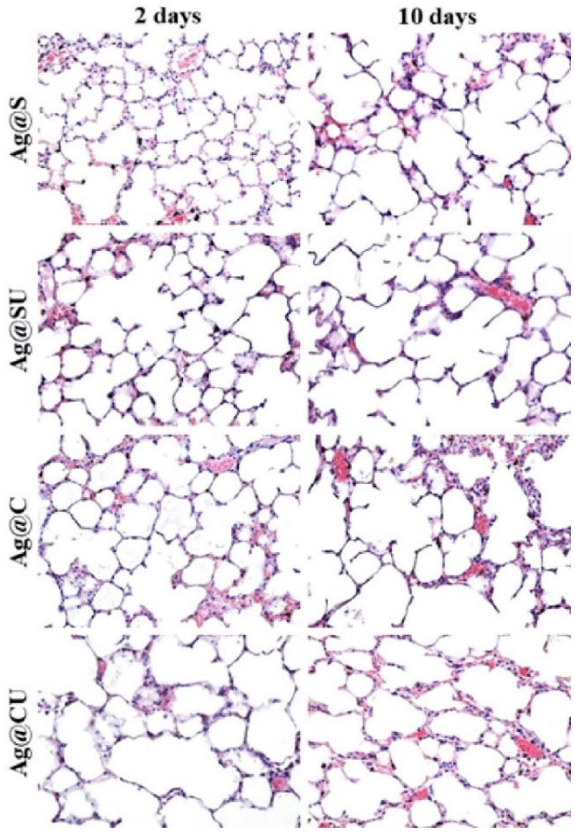

Figure 8 – ***Optical micrographs of pulmonary tissues after two and 10 days of treatment with Ag@EO NPs (HE staining, 200×). Ag@EO NPs: Essential oil-conjugated silver nanoparticles; HE: Hematoxylin–Eosin.***

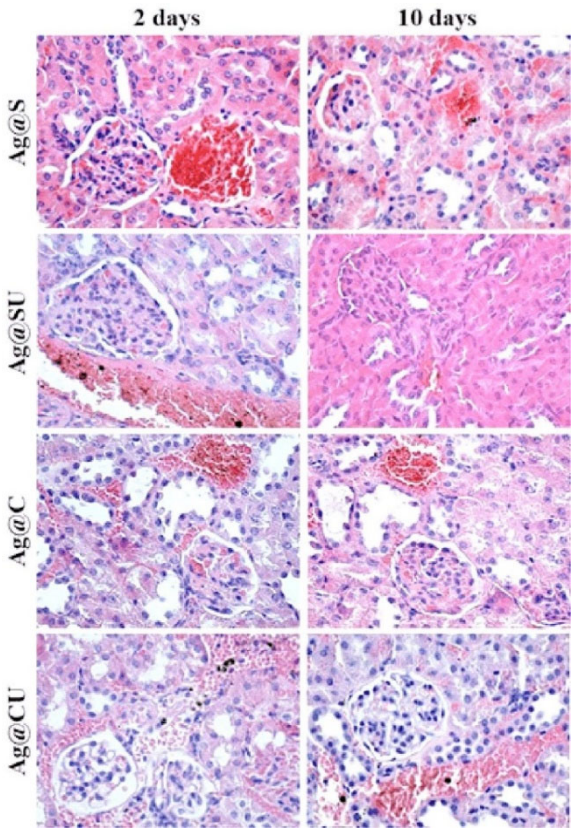

Figure 9 – ***Optical micrographs of renal tissues after two and 10 days of treatment with Ag@EO NPs (HE staining, 400×). Ag@EO NPs: Essential oil-conjugated silver nanoparticles; HE: Hematoxylin–Eosin.***

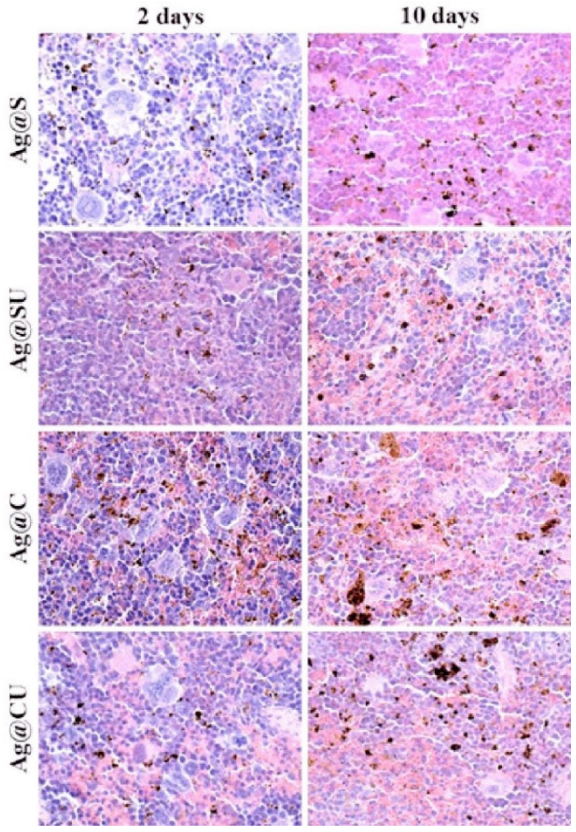

Figure 10 – ***Optical micrographs of splenic tissues after two and 10 days of treatment with Ag@EO NPs (HE staining, 400×). Ag@EO NPs: Essential oil-conjugated silver nanoparticles; HE: Hematoxylin–Eosin.***

Discussions

The attractive and versatile functionality of AgNPs enable their revaluation for the development of new and improved biomaterials, biomedical devices, and biotechnologies. Alongside size [53, 54] and morphology [55, 56], surface charge and reactivity [57, 58] are essential aspects responsible for specific interactions between AgNPs and cells, which determine tunable therapeutic effects.

Impressive efforts have been lately oriented towards the use of plant-derived phytochemicals, including EOs, for the development of unconventional and performance-enhanced therapeutic formulations.

Volatility and degradation are important drawbacks of EOs [59, 60], therefore the herein proposed Ag@EO NPs represent a dual strategy to (*i*) improve the compatibility and stability of metallic NPs by the conjugation of EO molecules and (*ii*) improve the stability of EOs through the inorganic core.

Sage and cinnamon EOs were selected in our study to obtain the Ag@EO NPs. The chemical reduction process was completed either under magnetic stirring (Ag@S, Ag@C) or sonochemical (Ag@SU, Ag@CU) conditions. Besides being versatile and facile processes, both synthesis strategies are efficient and reproducible, enable high yield synthesis and allow control over the size, morphology and surface chemistry of the final NPs in few steps or even one-step protocol [61, 62].

An early indicator on the successful AgNP synthesis was observed when the metallic precursor solution was added to the organic solution. A fast and gradual color

modification occurred, regardless of the process conditions (magnetic stirring or sonication). Dark-green and brown-green final suspensions were obtained when sage and cinnamon EOs were used, respectively. This observation was correlated with the reduction of Ag^+ to Ag^0 and, consequently, to the formation of Ag@EO NPs [63, 64].

The XRD analysis confirmed the high purity of synthesized samples and the presence of metallic Ag with fcc crystallographic lattice [65, 66] as the sole crystalline phase of obtained powders.

Regardless of the type of synthesis method, the thermal analysis revealed the predominant metallic character of NPs conjugated with sage EO (Ag@S, Ag@SU), whereas the use of cinnamon EO (Ag@C, Ag@CU) resulted in an increased amount of conjugated organic molecules. Current literature reports temperatures between 150–250ºC for complete volatilization and thermal decomposition of EOs [67–70]. Our TGA data proved the thermal stabilizing role of AgNPs on selected EOs.

SEM and TEM micrographs evidenced the formation of nanosized particles with preferential spherical morphology. No substantial dimensional differences were noticed between particles obtained either by magnetic stirring or ultrasound-assisted reduction. Core/shell NPs with physical size of ~25 nm (Ag@S), ~27 nm (Ag@SU), ~16 nm (Ag@C) and ~19 nm (Ag@CU) were evidenced.

In comparison with conventional reduction protocols, the sonochemical synthesis generally leads to the formation of smaller NPs due to cavitation effects, which determine faster and more intense reactions within transient "micro-reactors" (ultrasound-generated bubbles within the aqueous solution), thus limiting growth and encouraging nucleation processes [71, 72]. Besides being thicker, the organic layers formed in the case of Ag@SU and Ag@CU were more dense and compact, which proved the beneficial role of ultrasound cavitation for the dispersion of EO's molecules [73, 74] and resulted in a reduced particle aggregation. In contrast to other studies on the sono-chemical synthesis of AgNPs [75, 76], the particle size of Ag@SU and Ag@CU was slightly increased, when compared with Ag@EO NPs obtained by conventional reduction. We asserted that this particular situation was due to (*i*) the reduced intensity of acoustic waves generated by the ultrasonic bath in comparison with those generated by the sonication probe and (*ii*) the thicker EO layer formed onto the particles, as the HR-TEM evidenced a much smaller inorganic core and a significantly thicker organic layer for Ag@SU and Ag@CU than in the case of conventionally synthesized Ag@EO NPs.

Diffraction planes of fcc Ag were evidenced from SAED patterns, which was in compliance with XRD results and previous studies [77, 78]. Moreover, as the crystallite size estimated from XRD data was comparable with the particle size estimated from TEM results for all samples, we concluded that spherical monocrystalline Ag@EO NPs were successfully obtained in our study.

The histological evaluation of vital organs harvested after systemic administration of Ag@EO NPs revealed preferential tissue distribution. Regardless of the type of EO and synthesis conditions, the treatment with Ag@EO NPs did not induce structural or functional modifications within the mouse brain, myocardium or pancreas.

A time-dependent tissue distribution of Ag@EO NPs was noticed in the case of hepatic and pulmonary tissues. Dark-brown aggregates were identified within tissue-specific resident macrophages after both treatment times. As shown by TEM images, Ag@SU and Ag@CU NPs had a much thicker organic layer onto their surfaces which, consequently, determined reduced aggregation and increased stability. This observation could explain the presence of smaller aggregates after both treatments. The normal ultrastructure of hepatic tissues was not affected after the treatment with Ag@EO NPs. The liver accumulation of AgNPs coated with positively charged coatings was previously reported in a fish model, accompanied by size-related inflammation and genotoxicity [79, 80]. Toxic effects, evidenced by both liver inflammation and up-regulation of hepatotoxic markers, were reported for citrate-capped AgNPs [81]. Increased alveolar breakdown and inflammatory infiltrate were noticed after prolonged treatment with Ag@EO NPs. Increased pulmonary inflammatory infiltrate was also reported after treatment with AgNPs coated with citrate or polyvinylpyrrolidone. These treatments also caused time- and dose-depended ultrastructural and functional cardiovascular effects [apoptosis and oxidative deoxyribonucleic acid (DNA) damage in cardiomyocytes, coagulation alteration and thrombosis, respectively] [82].

Ag@EO NPs aggregates were evidenced within the blood vessels of renal fragments, but no morphological and ultrastructural alterations were identified at this level. The size and presence of such aggregates was significantly reduced after 10 days of treatment. Citrate-coated AgNPs were reported to alter kidney and liver functions in pregnant rats, accompanied by mild hepatic inflammation and minimal toxicity in fetuses [83].

Significant modifications were noticed within the spleen, after both testing times. A time-dependent presence of Ag@EO NPs aggregates was observed within the splenic red pulp, accompanied by the substantial hypertrophy of the splenic white pulp. The presence of AgNPs aggregates within spleen was previously reported after intravenous administration [84], but such aggregates were absent and normal histology of spleen was reported in the case of NPs coated with bacterial lactonase [85].

Conclusions

The development of safe and efficient AgNPs-based platforms for biomedical applications represents an attractive challenge, as the balance between cytocompatibility and therapeutic effects should be accurately and specifically tuned through their nanosize-related characteristics. Besides dimension and morphology, surface features of AgNPs play an essential role for the fabrication of new and effective pharmaceutical formulations. By using sage and cinnamon EOs, Ag@EO NPs were prepared within this study. Regardless of the synthesis process, which was performed either under magnetic stirring (Ag@S, Ag@C) or sonochemical (Ag@SU, Ag@CU) conditions, monocrystalline spherical NPs were obtained. Following their systemic administration in a BALB/c animal model, preferential tissue retention and biodistribution were revealed. The Ag@EO NPs were absent in the brain,

myocardium, and pancreas tissues. Their presence as aggregates was noticed within the hepatic and pulmonary tissues, with ultrastructure modifications being observed in the latter case. The presence of a more dense and thicker organic layer on the surface of the NPs obtained by ultrasound-assisted synthesis (Ag@SU, Ag@CU) determined reduced aggregation and resulted in less accumulation within these tissues. The presence of Ag@EO NPs aggregates was evidenced within the blood vessels of renal fragments, but no morphological and ultrastructural alterations were identified at this level. As expected, significant modifications were observed within the spleen, both after two and 10 days of treatment. By modifying and improving the surface of Ag@EO NPs, specific and non-toxic antimicrobial platforms for developing targeted treatment models against different ailments could be developed in the future.

Conflict of interests

The authors declare that they have no conflict of interests.

Acknowledgments

This work was supported by a grant of the Romanian Ministry of Research and Innovation, CCDI – UEFISCDI, project number PN-III-P1-1.2-PCCDI-2017-0749/45PCCDI/ 2018, within PNCDI III ("Bioactive nanostructures for innovative therapeutic strategies").

References

[1] Sharma N, Phutela K, Goel A, Soni S, Batra N. Exploring the bacterial based silver nanoparticle for their possible application as disinfectants. Biointerface Res Appl Chem 2018, 8(1): 3100–3104. https://biointerfaceresearch.com/?download=2225

[2] Montes de Oca-Vásquez G, Solano-Campos F, Vega-Baudrit JR, López-Mondéjar R, Vera A, Moreno JL, Bastida F. Organic amendments exacerbate the effects of silver nanoparticles on microbial biomass and community composition of a semiarid soil. Sci Total Environ, 2020, 744:140919. https://doi.org/10.1016/j.scitotenv.2020.140919 PMID: 32711321

[3] Lee SJ, Begildayeva T, Yeon S, Naik SS, Ryu H, Kim TH, Choi MY. Eco-friendly synthesis of lignin mediated silver nanoparticles as a selective sensor and their catalytic removal of aromatic toxic nitro compounds. Environ Pollut 2021, 269: 116174. https://doi.org/10.1016/j.envpol.2020.116174 PMID: 33280906

[4] Wang H, Xie H, Wang S, Gao Z, Li C, Hu GH, Xiong C. Enhanced dielectric property and energy storage density of PVDF-HFP based dielectric composites by incorporation of silver nanoparticles-decorated exfoliated montmorillonite nanoplatelets. Compos Part A Appl Sci Manuf, 2018, 108:62–68. https://doi.org/10.1016/j.compositesa.2018.02.020

[5] Ramanarayanan R, Chokiveetil N, Pullanjiyot N, Meethal BN, Swaminathan S. The deterministic role of resonance energy transfer in the performance of bio-inspired colloidal silver nanoparticles incorporated dye sensitized solar cells. Mater Res Bull, 2019, 114:28–36. https://doi.org/10.1016/j.materresbull.2019.02.017

[6] Pradeep N, Paramasivam K, Rajesh T, Subash Purusothamanan V, Iyahraja S. Silver nanoparticles for enhanced thermal energy storage of phase change materials. Mater Today Proc, 2020 March 17. https://doi.org/10.1016/j.matpr.2020.02.671

[7] Alshammari AS, Alenezi MR, Silva SRP. Excimer laser sintereing of silver nanoparticles electrodes for fully solution processed organic thin film transistors. Opt Laser Technol, 2019, 120:105758. https://doi.org/10.1016/j.optlastec.2019.105758

[8] Al-Masoodi AHH, Nazarudin NFFB, Nakajima H, Tunmee S, Goh BT, Majid WHBA. Controlled growth of silver nanoparticles on indium tin oxide substrates by plasma-assisted hot-filament evaporation: physical properties, composition, and electronic structure. Thin Solid Films, 2020, 693:137686. https://doi.org/10.1016/j.tsf.2019.137686

[9] Zhuo L, Liu W, Zhao Z, Yin E, Li C, Zhou L, Zhang Q, Feng Y, Lin S. Cost-effective silver nano-ink for inkjet printing in application of flexible electronic devices. Chem Phys Lett, 2020, 757:137904. https://doi.org/10.1016/j.cplett.2020.137904

[10] Tang J, Chen W, Ju H. Sensitive surface-enhanced Raman scattering detection of atrazine based on aggregation of silver nanoparticles modified carbon dots. Talanta, 2019, 201:46–51. https://doi.org/10.1016/j.talanta.2019.03.108 PMID: 31122450

[11] Hassanpour S, Hasanzadeh M, Saadati A, Shadjou N, Soleymani J, Jouyban A. A novel paper based immunoassay of breast cancer specific carbohydrate (CA 15.3) using silver nanoparticles-reduced graphene oxide nano-ink technology: a new platform to construction of microfluidic paper-based analytical devices (μPADs) towards biomedical analysis. Microchem J, 2019, 146:345–358. https://doi.org/10.1016/j.microc.2019.01.018

[12] Juang RS, Wang KS, Cheng YW, Fu CC, Chen WT, Liu CM, Chien CC, Jeng RJ, Chen CC, Liu TY. Floating SERS substrates of silver nanoparticles-graphene based nanosheets for rapid detection of biomolecules and clinical uremic toxins. Colloids Surf A Physicochem Eng Asp, 2019, 576:36–42. https://doi.org/10.1016/j.colsurfa.2019.05.042

[13] Samoilova NA, Krayukhina MA, Popov DA, Anuchina NM, Piskarev VE. 3'-Sialyllactose-decorated silver nanoparticles: lectin binding and bactericidal properties. Biointerface Res Appl Chem, 2018, 8(1):3095–3099. https://biointerfaceresearch.com/?download=2218

[14] Valsalam S, Agastian P, Esmail GA, Ghilan AKM, Al-Dhabi NA, Arasu MV. Biosynthesis of silver and gold nanoparticles using *Musa acuminata* Colla flower and its pharmaceutical activity against bacteria and anticancer efficacy. J Photochem Photobiol B Biol, 2019, 201:111670. https://doi.org/10.1016/j.jphotobiol.2019.111670

[15] Zhang X, Li Y, Hu Y. Green synthesis of silver nanoparticles and their preventive effect in deficits in recognition and spatial memory in sporadic Alzheimer's rat model. Colloids Surf A Physicochem Eng Asp, 2020, 605:125288. https://doi.org/10.1016/j.colsurfa.2020.125288

[16] Saini RK, Bagri LP, Bajpai AK. Nano-silver hydroxyapatite based antibacterial 3D scaffolds of gelatin/alginate/poly (vinyl alcohol) for bone tissue engineering applications. Colloids Surf B Biointerfaces, 2019, 177:211–218. https://doi.org/10.1016/j.colsurfb.2019.01.064 PMID: 30743068

[17] Grumezescu AM, Stoica AE, Dima-Bălcescu MŞ, Chircov C, Gharbia S, Baltă C, Roşu M, Herman H, Holban AM, Ficai A, Vasile BS, Andronescu E, Chifiriuc MC, Hermenean A. Electrospun polyethylene terephthalate nanofibers loaded with silver nanoparticles: novel approach in anti-infective therapy. J Clin Med, 2019, 8(7):1039. https://doi.org/10.3390/jcm8071039 PMID: 31315266 PMCID: PMC6679131

[18] Gherasim O, Grumezescu AM, Grumezescu V, Iordache F, Vasile BS, Holban AM. Bioactive surfaces of polylactide and silver nanoparticles for the prevention of microbial contamination. Materials (Basel), 2020, 13(3):768. https://doi.org/10.3390/ma13030768 PMID: 32046134 PMCID: PMC7040686

[19] Khan I, Bahuguna A, Krishnan M, Shukla S, Lee H, Min SH, Choi DK, Cho Y, Bajpai VK, Huh YS, Kang SC. The effect of biogenic manufactured silver nanoparticles on human endothelial cells and zebrafish model. Sci Total Environ, 2019, 679:365–377. https://doi.org/10.1016/j.scitotenv.2019.05.045 PMID: 31085416

[20] Tang J, Lu X, Chen B, Cai E, Liu W, Jiang J, Chen F, Shan X, Zhang H. Mechanisms of silver nanoparticles-induced cytotoxicity and apoptosis in rat tracheal epithelial cells. J Toxicol Sci, 2019, 44(3):155–165. https://doi.org/10.2131/jts.44.155 PMID: 30842368

[21] Bin-Jumah M, Al-Abdan M, Albasher G, Alarifi S. Effects of green silver nanoparticles on apoptosis and oxidative stress in normal and cancerous human hepatic cells *in vitro*. Int J Nanomedicine, 2020, 15:1537–1548. https://doi.org/10.2147/IJN.S239861 PMID: 32210550 PMCID: PMC7074819

[22] Sabry NM, Tolba S, Abdel-Gawad FK, Bassem SM, Nassar HF, El-Taweel GE, Okasha A, Ibrahim M. Interaction between nano silver and bacteria: modeling approach. Biointerface Res Appl Chem, 2018, 8(5):3570–3574. https://biointerfaceresearch.com/?download=2549

[23] Li WR, Sun TL, Zhou SL, Ma YK, Shi QS, Xie XB, Huang XM. A comparative analysis of antibacterial activity, dynamics, and effects of silver ions and silver nanoparticles against four bacterial strains. Int Biodeterior Biodegradation, 2017, 123:304–310. https://doi.org/10.1016/j.ibiod.2017.07.015
[24] Morris D, Ansar M, Speshock J, Ivanciuc T, Qu Y, Casola A, Garofalo R. Antiviral and immunomodulatory activity of silver nanoparticles in experimental RSV infection. Viruses, 2019, 11(8):732. https://doi.org/10.3390/v11080732 PMID: 31398832 PMCID: PMC6723559
[25] Pittol M, Tomacheski D, Simões DN, Ribeiro VF, Santana RMC. Evaluation of the toxicity of silver/silica and titanium dioxide particles in mammalian cells. Braz Arch Biol Technol, 2018, 61:e18160667. https://doi.org/10.1590/1678-4324-2018160667
[26] Mallakpour S, Abbasi M. Hydroxyapatite mineralization on chitosan-tragacanth gum/silica@silver nanocomposites and their antibacterial activity evaluation. Int J Biol Macromol, 2020, 151:909–923. https://doi.org/10.1016/j.ijbiomac.2020.02.167 PMID: 32084463
[27] Wang M, Li H, Li Y, Mo F, Li Z, Chai R, Wang H. Dispersibility and size control of silver nanoparticles with anti-algal potential based on coupling effects of polyvinylpyrrolidone and sodium tripolyphosphate. Nanomaterials (Basel), 2020, 10(6):1042. https://doi.org/10.3390/nano10061042 PMID: 32485998 PMCID: PMC7352764
[28] Martínez-Rodríguez MA, Madla-Cruz E, Urrutia-Baca VH, de la Garza-Ramos MA, González-González VA, Garza-Navarro MA. Influence of polysaccharides' molecular structure on the antibacterial activity and cytotoxicity of green synthesized composites based on silver nanoparticles and carboxymethylcellulose. Nanomaterials (Basel), 2020, 10(6):1164. https://doi.org/10.3390/nano10061164 PMID: 32545858 PMCID: PMC7353245
[29] Keshvadi M, Karimi F, Valizadeh S, Valizadeh A. Comparative study of antibacterial inhibitory effect of silver nanoparticles and garlic oil nanoemulsion with their combination. Biointerface Res Appl Chem, 2019, 9(6):4560–4566. https://doi.org/10.33263/BRIAC96.560566
[30] Abd El-Hady MM, Saeed SES. Antibacterial properties and pH sensitive swelling of *in situ* formed silver–curcumin nanocomposite based chitosan hydrogel. Polymers (Basel), 2020, 12(11):2451. https://doi.org/10.3390/polym12112451 PMID: 33114003 PMCID: PMC7690720
[31] Jung J, Raghavendra GM, Kim D, Seo J. One-step synthesis of starch-silver nanoparticle solution and its application to antibacterial paper coating. Int J Biol Macromol, 2018, 107(Pt B):2285–2290. https://doi.org/10.1016/j.ijbiomac.2017.10.108 PMID: 29054526
[32] Francesko A, Cano Fossas M, Petkova P, Fernandes MM, Mendoza E, Tzanov T. Sonochemical synthesis and stabilization of concentrated antimicrobial silver–chitosan nanoparticle dispersions. J Appl Polym Sci, 2017, 134(30):45136. https://doi.org/10.1002/app.45136
[33] Mahjouri S, Movafeghi A, Divband B, Kosari-Nasab M, Kazemi EM. Assessing the toxicity of silver nanoparticles in cell suspension culture of *Nicotiana tabacum*. Biointerface Res Appl Chem, 2018, 8(3):3252–3258. https://biointerfaceresearch.com/?download=2350
[34] Lopes CRB, Courrol LC. Green synthesis of silver nanoparticles with extract of *Mimusops coriacea* and light. J Lumin, 2018, 199:183–187. https://doi.org/10.1016/j.jlumin.2018.03.030
[35] Dhayagude AC, Das A, Joshi SS, Kapoor S. *γ*-Radiation induced synthesis of silver nanoparticles in aqueous poly (*N*-vinylpyrrolidone) solution. Colloids Surf A Physicochem Eng Asp, 2018, 556:148–156. https://doi.org/10.1016/j.colsurfa.2018.08.028
[36] Ali GW, Abd El-Moez ShI, Abdel-Fattah WA. Synthesis and characterization of nontoxic silver nano-particles with preferential bactericidal activity. Biointerface Res Appl Chem, 2019, 9(6):4617–4623. https://doi.org/10.33263/BRIAC96.617623
[37] Rodrigues dos Santos LD, Soares dos Santos AE, Penna Cerávolo I, Barbosa Figueiredo FJ, Dias-Souza MV. Antibiofilm activity of black tea leaf extract, its cytotoxicity and interference on the activity of antimicrobial drugs. Biointerface Res Appl Chem, 2018, 8(5):3565–3569. https://biointerfaceresearch.com/?download=2546
[38] Negut I, Grumezescu V, Ficai A, Grumezescu AM, Holban AM, Popescu RC, Savu D, Vasile BS, Socol G. MAPLE deposition of *Nigella sativa* functionalized Fe_3O_4 nanoparticles for antimicrobial coatings. Appl Surf Sci, 2018, 455:513–521. https://doi.org/10.1016/j.apsusc.2018.05.202
[39] Shetta A, Kegere J, Mamdouh W. Comparative study of encapsulated peppermint and green tea essential oils in chitosan nanoparticles: encapsulation, thermal stability, *in-vitro* release, antioxidant and antibacterial activities. Int J Biol Macromol, 2019, 126:731–742. https://doi.org/10.1016/j.ijbiomac.2018.12.161 PMID: 30593811
[40] Hamedi A, Zengin G, Aktumsek A, Selamoglu Z, Pasdaran A. *In vitro* and *in silico* approach to determine neuroprotective properties of iridoid glycosides from aerial parts of *Scrophularia amplexicaulis* by investigating their cholinesterase inhibition and anti-oxidant activities. Biointerface Res Appl Chem, 2020, 10(3):5429–5454. https://doi.org/10.33263/BRIAC103.429454
[41] Jabir MS, Taha AA, Sahib UI, Taqi ZJ, Al-Shammari AM, Salman AS. Novel of nano delivery system for Linalool loaded on gold nanoparticles conjugated with CALNN peptide for application in drug uptake and induction of cell death on breast cancer cell line. Mater Sci Eng C Mater Biol Appl, 2019, 94:949–964. https://doi.org/10.1016/j.msec.2018.10.014 PMID: 30423784
[42] Arzani H, Adabi M, Mosafer J, Dorkoosh F, Khosravani M, Maleki H, Nekounam H, Kamali M. Preparation of curcumin-loaded PLGA nanoparticles and investigation of its cytotoxicity effects on human glioblastoma U87MG cells. Biointerface Res Appl Chem, 2019, 9(5):4225–4231. https://doi.org/10.33263/BRIAC95.225231
[43] Balaure PC, Holban AM, Grumezescu AM, Mogoşanu GD, Bălşeanu TA, Stan MS, Dinischiotu A, Volceanov A, Mogoantă L. *In vitro* and *in vivo* studies of novel fabricated bioactive dressings based on collagen and zinc oxide 3D scaffolds. Int J Pharm, 2019, 557:199–207. https://doi.org/10.1016/j.ijpharm.2018.12.063 PMID: 30597267
[44] Amanzadi B, Mirzaei E, Hassanzadeh G, Mahdaviani P, Boroumand S, Abdollahi M, Abdolghaffari AH, Majidi RF. Chitosan-based layered nanofibers loaded with herbal extract as wound-dressing materials on wound model studies. Biointerface Res Appl Chem, 2019, 9(4):3979–3986. https://doi.org/10.33263/BRIAC94.979986
[45] Popa M, Măruţescu L, Oprea E, Bleotu C, Kamerzan C, Chifiriuc MC, Grădişteanu Pircalabioru G. *In vitro* evaluation of the antimicrobial and immunomodulatory activity of culinary herb essential oils as potential perioceutics. Antibiotics (Basel), 2020, 9(7):428. https://doi.org/10.3390/antibiotics9070428 PMID: 32708120 PMCID: PMC7399839
[46] Yazgan H. Investigation of antimicrobial properties of sage essential oil and its nanoemulsion as antimicrobial agent. LWT, 2020, 130:109669. https://doi.org/10.1016/j.lwt.2020.109669
[47] Pejčić M, Stojanović-Radić Z, Genčić M, Dimitrijević M, Radulović N. Anti-virulence potential of basil and sage essential oils: inhibition of biofilm formation, motility and pyocyanin production of *Pseudomonas aeruginosa* isolates. Food Chem Toxicol, 2020, 141:111431. https://doi.org/10.1016/j.fct.2020.111431 PMID: 32417365
[48] Soto-Chilaca GA, Mejía-Garibay B, Navarro-Amador R, Ramírez-Corona N, Palou E, López-Malo A. Cinnamaldehyde-loaded chitosan nanoparticles: characterization and antimicrobial activity. Biointerface Res Appl Chem, 2019, 9(4):4060–4065. https://doi.org/10.33263/BRIAC94.060065
[49] Chuesiang P, Siripatrawan U, Sanguandeekul R, McClements DJ, McLandsborough L. Antimicrobial activity of PIT-fabricated cinnamon oil nanoemulsions: effect of surfactant concentration on morphology of foodborne pathogens. Food Control, 2019, 98:405–411. https://doi.org/10.1016/j.foodcont.2018.11.024
[50] Saki M, Seyed-Mohammadi S, Montazeri EA, Siahpoosh A, Moosavian M, Latifi SM. *In vitro* antibacterial properties of *Cinnamomum zeylanicum* essential oil against clinical extensively drug-resistant bacteria. Eur J Integr Med, 2020, 37:101146. https://doi.org/10.1016/j.eujim.2020.101146
[51] Albeladi SSR, Malik MA, Al-thabaiti SA. Facile biofabrication of silver nanoparticles using *Salvia officinalis* leaf extract and its catalytic activity towards Congo red dye degradation. J Mater Res Technol, 2020, 9(5):10031–10044. https://doi.org/10.1016/j.jmrt.2020.06.074
[52] González-Rivera J, Duce C, Falconieri D, Ferrari C, Ghezzi L, Piras A, Tine MR. Coaxial microwave assisted hydrodistillation

of essential oils from five different herbs (lavender, rosemary, sage, fennel seeds and clove buds): chemical composition and thermal analysis. Innov Food Sci Emerg Technol, 2016, 33:308–318. https://doi.org/10.1016/j.ifset.2015.12.011

[53] Ji H, Zhou S, Fu Y, Wang Y, Mi J, Lu T, Wang X, Lü C. Size-controllable preparation and antibacterial mechanism of thermo-responsive copolymer-stabilized silver nanoparticles with high antimicrobial activity. Mater Sci Eng C Mater Biol Appl, 2020, 110:110735. https://doi.org/10.1016/j.msec.2020.110735 PMID: 32204045

[54] Zhang B, Liu N, Liu QS, Zhang J, Zhou Q, Jiang G. Silver nanoparticles induce size-dependent and particle-specific neurotoxicity to primary cultures of rat cerebral cortical neurons. Ecotoxicol Environ Saf, 2020, 198:110674. https://doi.org/10.1016/j.ecoenv.2020.110674 PMID: 32387843

[55] Ali S, Perveen S, Ali M, Jiao T, Sharma AS, Hassan H, Devaraj S, Li H, Chen Q. Bioinspired morphology-controlled silver nanoparticles for antimicrobial application. Mater Sci Eng C Mater Biol Appl, 2020, 108:110421. https://doi.org/10.1016/j.msec.2019.110421 PMID: 31923969

[56] Graf C, Nordmeyer D, Sengstock C, Ahlberg S, Diendorf J, Raabe J, Epple M, Köller M, Lademann J, Vogt A, Rancan F, Rühl E. Shape-dependent dissolution and cellular uptake of silver nanoparticles. Langmuir, 2018, 34(4):1506–1519. https://doi.org/10.1021/acs.langmuir.7b03126 PMID: 29272915

[57] Kim DH, Park JC, Jeon GE, Kim CS, Seo JH. Effect of the size and shape of silver nanoparticles on bacterial growth and metabolism by monitoring optical density and fluorescence intensity. Biotechnol Bioprocess Eng, 2017, 22(2):210–217. https://doi.org/10.1007/s12257-016-0641-3

[58] Zucker RM, Ortenzio J, Degn LL, Lerner JM, Boyes WK. Biophysical comparison of four silver nanoparticles coatings using microscopy, hyperspectral imaging and flow cytometry. PLoS One, 2019, 14(7):e0219078. https://doi.org/10.1371/journal.pone.0219078 PMID: 31365549 PMCID: PMC6668787

[59] Yazgan H, Ozogul Y, Kuley E. Antimicrobial influence of nanoemulsified lemon essential oil and pure lemon essential oil on food-borne pathogens and fish spoilage bacteria. Int J Food Microbiol, 2019, 306:108266. https://doi.org/10.1016/j.ijfoodmicro.2019.108266 PMID: 31319195

[60] Jiang Y, Wang D, Li F, Li D, Huan Q. Cinnamon essential oil Pickering emulsion stabilized by zein–pectin composite nanoparticles: characterization, antimicrobial effect and advantages in storage application. Int J Biol Macromol, 2020, 148:1280–1289. https://doi.org/10.1016/j.ijbiomac.2019.10.103 PMID: 31739045

[61] Amini E, Azadfallah M. *In situ* synthesis of silver nanoparticles on fiber matrix for preparing antibacterial paper. Biointerface Res Appl Chem, 2018, 8(4):3449–3456. https://biointerfaceresearch.com/?download=2463

[62] Eze FN, Nwabor OF. Valorization of *Pichia* spent medium *via* one-pot synthesis of biocompatible silver nanoparticles with potent antioxidant, antimicrobial, tyrosinase inhibitory and reusable catalytic activities. Mater Sci Eng C Mater Biol Appl, 2020, 115:111104. https://doi.org/10.1016/j.msec.2020.111104 PMID: 32600707

[63] Narasaiah BP, Mandal BK, Chakravarthula SN. Mitigation of textile industries generated pollution by agro-waste cotton peels mediated synthesized silver nanoparticles. Biointerface Res Appl Chem, 2018, 8(5):3602–3610. https://biointerfaceresearch.com/?download=2564

[64] Pirtarighat S, Ghannadnia M, Baghshahi S. Green synthesis of silver nanoparticles using the plant extract of *Salvia spinosa* grown *in vitro* and their antibacterial activity assessment. J Nanostructure Chem, 2019, 9(1):1–9. https://doi.org/10.1007/s40097-018-0291-4

[65] Aziz SB, Hussein G, Brza MA, Mohammed SJ, Abdulwahid RT, Saeed SR, Hassanzadeh A. Fabrication of interconnected plasmonic spherical silver nanoparticles with enhanced localized surface plasmon resonance (LSPR) peaks using quince leaf extract solution. Nanomaterials, 2019, 9(11):1557. https://doi.org/10.3390/nano9111557 PMID: 31684041 PMCID: PMC6915396

[66] Azmi AA, Ahyat N, Mohamad F, Hamzah S. Synthesis of silver nanoparticles: double-green approach of using chitosan and microwave technique towards antimicrobial activity against pathogenic bacteria. Biointerface Res Appl Chem, 2020, 10(4):5918–5922. https://doi.org/10.33263/briac104.918922

[67] Duce C, Ciprioti SV, Spepi A, Bernazzani L, Tinè MR. Vaporization kinetic study of lavender and sage essential oils. J Therm Anal Calorim, 2017, 130(1):595–604. https://doi.org/10.1007/s10973-017-6503-1

[68] Micić D, Ostojić S, Pezo L, Blagojević S, Pavlić B, Zeković Z, Đurović S. Essential oils of coriander and sage: investigation of chemical profile, thermal properties and QSRR analysis. Ind Crops Prod, 2019, 138:111438. https://doi.org/10.1016/j.indcrop.2019.06.001

[69] Muhoza B, Xia S, Cai J, Zhang X, Duhoranimana E, Su J. Gelatin and pectin complex coacervates as carriers for cinnamaldehyde: effect of pectin esterification degree on coacervate formation, and enhanced thermal stability. Food Hydrocoll, 2019, 87:712–722. https://doi.org/10.1016/j.foodhyd.2018.08.051

[70] da Silva Barbosa RF, Yudice EDC, Mitra SK, dos Santos Rosa D. Characterization of Rosewood and Cinnamon *Cassia* essential oil polymeric capsules: stability, loading efficiency, release rate and antimicrobial properties. Food Control, 2021, 121:107605. https://doi.org/10.1016/j.foodcont.2020.107605

[71] Nouri A, Yaraki MT, Lajevardi A, Rezaei Z, Ghorbanpour M, Tanzifi M. Ultrasonic-assisted green synthesis of silver nanoparticles using *Mentha aquatica* leaf extract for enhanced antibacterial properties and catalytic activity. Colloid Interface Sci Commun, 2021, 35:100252. https://doi.org/10.1016/j.colcom.2020.100252

[72] Fuentes-García JA, Santoyo-Salzar J, Rangel-Cortes E, Goya GF, Cardozo-Mata V, Pescador-Rojas DA. Effect of ultrasonic irradiation power on sonochemical synthesis of gold nanoparticles. Ultrason Sonochem, 2021, 70:105274. https://doi.org/10.1016/j.ultsonch.2020.105274

[73] Yan Q, Qiu M, Chen X, Fan Y. Ultrasound assisted synthesis of size-controlled aqueous colloids for the fabrication of nanoporous zirconia membrane. Front Chem, 2019, 7:337. https://doi.org/10.3389/fchem.2019.00337 PMID: 31179266 PMCID: PMC6538813

[74] Guzmán K, Kumar B, Vallejo MJ, Grijalva M, Debut A, Cumbal L. Ultrasound-assisted synthesis and antibacterial activity of gallic acid–chitosan modified silver nanoparticles. Prog Org Coat, 2019, 129:229–235. https://doi.org/10.1016/j.porgcoat.2019.01.009

[75] Deshmukh AR, Gupta A, Kim BS. Ultrasound assisted green synthesis of silver and iron oxide nanoparticles using fenugreek seed extract and their enhanced antibacterial and antioxidant activities. BioMed Res Int, 2019, 2019:1714358. https://doi.org/10.1155/2019/1714358 PMID: 31080808 PMCID: PMC6476140

[76] Fatimah I, Hidayat H, Nugroho BH, Husein S. Ultrasound-assisted biosynthesis of silver and gold nanoparticles using *Clitoria ternatea* flower. S Afr J Chem Eng, 2020, 34:97–106. https://doi.org/10.1016/j.sajce.2020.06.007

[77] Yu C, Tang J, Liu X, Ren X, Zhen M, Wang L. Green biosynthesis of silver nanoparticles using *Eriobotrya japonica* (Thunb.) leaf extract for reductive catalysis. Materials (Basel), 2019, 12(1):189. https://doi.org/10.3390/ma12010189 PMID: 30626021 PMCID: PMC6337669

[78] Neacsu IA, Leau SA, Marin S, Holban AM, Vasile BS, Nicoara AI, Ene VL, Bleotu C, Albu Kaya MG, Ficai A. Collagen–carboxymethylcellulose biocomposite wound-dressings with antimicrobial activity. Materials (Basel), 2021, 14(5):1153. https://doi.org/10.3390/ma14051153 PMID: 33804421 PMCID: PMC7957653

[79] Liu H, Wang X, Wu Y, Hou J, Zhang S, Zhou N, Wang X. Toxicity responses of different organs of zebrafish (*Danio rerio*) to silver nanoparticles with different particle sizes and surface coatings. Environ Pollut, 2019, 264:414–422. https://doi.org/10.1016/j.envpol.2018.12.034

[80] Auclair J, Turcotte P, Gagnon C, Peyrot C, Wilkinson KJ, Gagné F. The influence of surface coatings on the toxicity of silver nanoparticle in rainbow trout. Comp Biochem Physiol C Toxicol Pharmacol, 2019, 226:108623. https://doi.org/10.1016/j.cbpc.2019.108623

[81] Jarrar Y, Al-Doaiss A, Alfaifi M, Shati A, Al-Kahtani M, Jarrar B. The influence of five metallic nanoparticles on the expression of major drug-metabolizing enzyme genes with correlation of inflammation in mouse livers. Environ Toxicol Pharmacol, 2020, 80:103449. https://doi.org/10.1016/j.etap.2020.103449

[82] Ferdous Z, Nemmar A. Health impact of silver nanoparticles: a review of the biodistribution and toxicity following various routes of exposure. Int J Mol Sci, 2020, 21(7):2375. https://doi.org/10.3390/ijms21072375 PMID: 32235542 PMCID: PMC7177798
[83] Elsharawy K, Abou-Dobara M, El-Gammal H, Hyder A. Chitosan coating does not prevent the effect of the transfer of green silver nanoparticles biosynthesized by *Streptomyces malachitus* into fetuses *via* the placenta. Reprod Biol, 2020, 20(1):97–105. https://doi.org/10.1016/j.repbio.2020.01.004 PMID: 32044208
[84] Fufă O, Andronescu E, Grumezescu V, Holban AM, Mogoantă L, Mogoşanu GD, Socol G, Iordache F, Chifiriuc MC, Grumezescu AM. Silver nanostructurated surfaces prepared by MAPLE for biofilm prevention. Biointerface Res Appl Chem, 2015, 5(6):1011–1017. https://biointerfaceresearch.com/?download=1146
[85] Gupta K, Chhibber S. Biofunctionalization of silver nanoparticles with lactonase leads to altered antimicrobial and cytotoxic properties. Front Mol Biosci, 2019, 6:63. https://doi.org/10.3389/fmolb.2019.00063 PMID: 31448285 PMCID: PMC6691173

Corresponding author
Alexandru Mihai Grumezescu, Associate Professor, Eng, PhD, Department of Science and Engineering of Oxide Materials and Nanomaterials, Faculty of Applied Chemistry and Materials Science, Politehnica University of Bucharest, 1–7 Gheorghe Polizu Street, Sector 1, 011061 Bucharest, Romania; Phone +4021–402 38 52, e-mail: grumezescu@yahoo.com

Received: January 10, 2021

Accepted: April 25, 2021